



University of Warwick institutional repository: <http://go.warwick.ac.uk/wrap>

This paper is made available online in accordance with publisher policies. Please scroll down to view the document itself. Please refer to the repository record for this item and our policy information available from the repository home page for further information.

To see the final version of this paper please visit the publisher's website. Access to the published version may require a subscription.

Author(s): K. Beuermann, F. Euchner, K. Reinsch, S. Jordan, B. T. Gänsicke

Article Title: Zeeman tomography of magnetic white dwarfs - IV. The complex field structure of the polars EF Eridani, BL Hydri and CP Tucanae

Year of publication: 2007

Link to published article:

<http://dx.doi.org/10.1051/0004-6361:20066332>

Publisher statement: © ESO 2007. Beuermann, K. et al. (2007).

Zeeman tomography of magnetic white dwarfs - IV. The complex field structure of the polars EF Eridani, BL Hydri and CP Tucanae.

Astronomy & Astrophysics, Vol.463 (2), pp.647-655

# Zeeman tomography of magnetic white dwarfs

## IV. The complex field structure of the polars EF Eridani, BL Hydri and CP Tucanae<sup>\*</sup>

K. Beuermann<sup>1</sup>, F. Euchner<sup>1, \*\*</sup>, K. Reinsch<sup>1</sup>, S. Jordan<sup>2</sup>, and B. T. Gänsicke<sup>3</sup>

<sup>1</sup> Institut für Astrophysik, Universität Göttingen, Friedrich-Hund-Platz 1, 37077 Göttingen, Germany  
e-mail: beuermann@astro.physik.uni-goettingen.de

<sup>2</sup> Astronomisches Rechen-Institut am ZAH, Mönchhofstr. 12–14, 69120 Heidelberg, Germany  
e-mail: jordan@ari.uni-heidelberg.de

<sup>3</sup> Department of Physics, University of Warwick, Coventry CV4 7AL, UK  
e-mail: Boris.Gaensicke@warwick.ac.uk

Received 1 September 2006 / Accepted 26 September 2006

### ABSTRACT

**Context.** The magnetic fields of the accreting white dwarfs in magnetic cataclysmic variables (mCVs) determine the accretion geometries, the emission properties, and the secular evolution of these objects.

**Aims.** We determine the structure of the surface magnetic fields of the white dwarf primaries in magnetic CVs using Zeeman tomography.

**Methods.** Our study is based on orbital-phase resolved optical flux and circular polarization spectra of the polars EF Eri, BL Hyi, and CP Tuc obtained with FORS1 at the ESO VLT. An evolutionary algorithm is used to synthesize best fits to these spectra from an extensive database of pre-computed Zeeman spectra. The general approach has been described in previous papers of this series.

**Results.** The results achieved with simple geometries as centered or offset dipoles are not satisfactory. Significantly improved fits are obtained for multipole expansions that are truncated at degree  $l_{\max} = 3$  or 5 and include all tesseral and sectoral components with  $0 \leq m \leq l$ . The most frequent field strengths of 13, 18, and 10 MG for EF Eri, BL Hyi, and CP Tuc, and the ranges of field strength covered are similar for the dipole and multipole models, but only the latter provide access to accreting matter at the right locations on the white dwarf. The results suggest that the field geometries of the white dwarfs in short-period mCVs are quite complex, with strong contributions from multipoles higher than the dipole in spite of a typical age of the white dwarfs in CVs in excess of 1 Gyr.

**Conclusions.** It is feasible to derive the surface field structure of an accreting white dwarf from phase-resolved low-state circular spectropolarimetry of sufficiently high signal-to-noise ratio. The fact that independent information is available on the strength and direction of the field in the accretion spot from high-state observations helps in unraveling the global field structure.

**Key words.** stars: white dwarfs – stars: magnetic fields – stars: atmospheres – polarization

### 1. Introduction

The subclass of magnetic cataclysmic variables (mCVs) termed polars (Krzesinski & Serkowski 1977) contains an accreting white dwarf that emits circularly polarized cyclotron radiation from an accretion region standing off the photosphere, often referred to as an accretion spot. The harmonic structure of the cyclotron radiation allows a straightforward measurement of the magnetic field and an estimate of the field direction in the spot. Photospheric absorption lines are heavily veiled by the intense cyclotron emission in the high (accreting) state. The field structure over the surface of the white dwarf becomes accessible to measurement only in low states of discontinued accretion via the profiles of the photospheric Zeeman-broadened Balmer absorption lines, an approach that is also applicable to non-accreting

isolated white dwarfs. Different from the latter, accreting systems offer the advantage that the strength and direction of the field in the accretion spot and its approximate location on the surface as determined from high-state observations represent a fixed point for the field structure. For simplicity it was often assumed that the field is quasi-dipolar, although accreting systems with two accretion spots separated by much less than 180° supported suspicions of a more complex structure (Meggitt & Wickramasinghe 1989; Pirola et al. 1987b; see Wickramasinghe & Ferrario 2000 for a review).

We have set out on a program to obtain a more complete picture of the surface field structure of magnetic white dwarfs using an approach dubbed Zeeman tomography (Euchner et al. 2002). The field geometries of two isolated white dwarfs, HE 1045-0908 and PG 1015+014 (Euchner et al. 2005, 2006), proved to be significantly more complex than simple centered or offset dipoles. In this paper, we present first results of the Zeeman tomography of three polars observed in their low states, EF Eri, BL Hyi, and CP Tuc, and find that they, too, have rather complex field geometries.

<sup>\*</sup> Based on observations collected at the European Southern Observatory, Paranal, Chile, under programme IDs 63.P-0003(A), 64.P-0150(C), and 66.D-0128(B).

<sup>\*\*</sup> Present address: Swiss Seismological Service, ETH Hönggerberg, 8093 Zürich, Switzerland.

**Table 1.** Dates of the spectropolarimetric observations obtained at the ESO VLT, exposure times, and number of exposures.

Object	Date	UT	$t_{\text{exp}}$ (s)	Number
EF Eri	2000/11/22	01:02–03:03	360	14
		04:24–05:14	360	6
BL Hyi	1999/12/04	04:25–06:29	360	16
CP Tuc	1999/06/04	08:07–08:44	480	4
		09:35–10:31	480	6

## 2. Observations and data analysis

We have obtained spin phase-resolved circular spectropolarimetry of EF Eri, BL Hyi, and CP Tuc in their low states. These stars belong to the short-period variety with orbital periods of 81.0 min (EF Eri), 113.6 min (BL Hyi), and 89.0 min (CP Tuc). The secondary star is a late M-star in BL Hyi. It is substellar in EF Eri (Beuermann et al. 2000; Harrison et al. 2004) and possibly in CP Tuc, too. Full orbital coverage was achieved for EF Eri and BL Hyi, but for technical reasons only half of the orbital period was covered for CP Tuc.

The data were collected at the ESO VLT using the focal reducer spectrograph FORS1. The instrument was operated in spectropolarimetric (PMOS) mode, with the GRIS\_300V+10 grism and an order separation filter GG 375, yielding a usable wavelength range of 3750–8450 Å. With a slit width of 1'', the *FWHM* spectral resolution was 13 Å at 5500 Å. A signal-to-noise ratio of typically  $S/N \approx 100$  was reached for the individual flux spectra. FORS1 contains a Wollaston prism for beam separation and two superachromatic phase retarder plate mosaics. Since both plates cannot be used simultaneously, only the circular polarization has been recorded using the quarter wave plate. Spectra of the target star and comparison stars in the field have been obtained simultaneously by using the multi-object spectroscopy mode of FORS1. This allows us to derive individual correction functions for the atmospheric absorption losses in the target spectra and to check for remnant instrumental polarization. Table 1 contains a log of the observations.

The observational data have been reduced according to standard procedures (bias, flat field, night sky subtraction, wavelength calibration, atmospheric extinction, flux calibration) using the context MOS of the ESO MIDAS package. To eliminate observational biases caused by Stokes parameter crosstalk, the wavelength-dependent degree of circular polarization  $V/I$  has been computed from two consecutive exposures recorded with the quarter wave retarder plate rotated by  $\pm 45^\circ$ . The circular polarization was then obtained as the average of two consecutive sets of spectra in the ordinary and the extraordinary beams (see Euchner et al. 2005, for details).

The three stars were in their low states with magnitudes estimated from the spectrophotometry of  $V \sim 18$  for EF Eri and BL Hyi and  $V \sim 19$  for CP Tuc. CCD photometry of BL Hyi in the same night gave  $V = 17.45$ . In the case of BL Hyi, the resulting spectra were corrected for the contribution by the secondary star using a spectrum of the dM5.5 star Gl 473 as a template. No trace of the secondary star was seen in the other two objects. Seeing variations and a loss of blue flux in the first two hours of the EF Eri run and in the last three spectra of BL Hyi affected the detection of orbital modulations. The orbital modulation of EF Eri seen in the remainder of the data is consistent with that reported by Szkody et al. (2006, and references therein). No substantial orbital modulation was detected in the data of BL Hyi and CP Tuc.

To facilitate analysis of the Zeeman absorption features, the continua of the observed spectra were normalized by the following procedure, which minimizes the differences between observed and theoretical continua, and also corrects for the mentioned loss of blue light. In a first step, a mean effective temperature of each object was determined by fitting a magnetic model spectrum to the quasi-continuum of the mean of the observed spectra unaffected by light loss. In a second step, the continua of all observed flux spectra were sampled in some 20 narrow fiducial wavelength intervals, which avoid the known Zeeman features and the emission lines, and adjusted to the best-fitting model spectrum using low-order polynomials (see Euchner et al. 2005, for more details). This approach removes the time variability in the flux continua, but leaves the equivalent widths of the Zeeman features largely unaffected. The mean effective temperature is  $T_{\text{eff}} = 11\,000$  K for EF Eri, 12000 K for BL Hyi, and 10000 K for CP Tuc, with an estimated accuracy of about  $\sim 1500$  K. Using this mean temperature in the tomographic analysis affects the theoretical Zeeman absorption features only minimally, because their equivalent width reaches a maximum around 11000 K and varies little with effective temperature around the maximum. In passing we note that our mean effective temperatures confirm the rather low temperatures of the white dwarfs in polars (Araujo-Betancor et al. 2005, and references therein). For the tomographic analysis, the flux and polarization spectra were collected into  $n = 4$  phase bins for EF Eri and  $n = 5$  for BL Hyi about equally spaced to cover the whole orbit. The spectra from the half orbit of CP Tuc were gathered into three bins.

## 3. General approach

We determine the global surface magnetic field structure using the Zeeman tomographic procedure described by Euchner et al. (2002, 2005, 2006). The process involves the inversion of the one-dimensional time series of rotational phase-resolved Zeeman flux and circular polarization spectra obtained in a non-accreting (low) state into a two-dimensional field distribution over the surface of the star. Because of the finite signal-to-noise ratio, this inversion problem may allow more than one solution within the observational uncertainties (for a discussion see Euchner et al. 2002). This ambiguity arises from the fact that different models may have similar frequency distributions of the field strength  $B$  and the angle  $\psi$  between field vector and line of sight and, hence, yield similar Zeeman spectra, but differ in the arrangement of the field over the surface. In this situation, it is advantageous to use the field vector in the accretion spot as deduced from cyclotron spectroscopy and broad band circular polarimetry in a high state as a fixpoint and effective constraint on the tomographic procedure. In the present paper, we have not included such a constraint in a formal way, but use it to select between solutions of the tomographic process obtained for different assumptions on the field geometry. To this end, we follow the surface field outward and determine the maximal radial distance reached by each field line. Field lines extending to more than  $R_{\text{max}} = 10 R_{\text{WD}}$  are considered 'open'. The accretion stream can couple to field lines which reach out sufficiently far, with the actual radius at which coupling can occur depending on the ram pressure of the accreting matter and the local field strength. The requirement that field lines that originate at a specific point at the surface reach out to more than several white dwarf radii can effectively discriminate between different field models. To be sure, a model that provides a good fit to the Zeeman spectra and possesses field lines reaching far out at the required position may not

be the correct model, but is as close to reality as we can presently get. As a further caveat, note that the actual coupling conditions have not been investigated and part of the far-reaching field lines may not be accessible to the stream. Consequently, only a fraction of the long ribbon-like structures of far-reaching field lines that appear in some models may act as foot points of accreting field lines. Nevertheless, with this information included, the analysis of accreting white dwarfs may yield more definite results than that of isolated white dwarfs.

As in our previous papers on isolated white dwarfs (Euchner et al. 2005, 2006), we fit the data with either a hybrid model or a multipole expansion truncated at a maximum degree  $l = l_{\max}$  including all  $l_{\max}(l_{\max} + 2)$  components with  $m = 0 \dots l$ . As a hybrid model, we consider the superposition of zonal ( $m = 0$ ) multipole components that are allowed to be inclined to each other and to be offset from the center of the white dwarf. Examples are, e.g., an offset dipole or the sum of dipole and quadrupole etc. Such combinations can easily be visualized given the polar field strengths and orientations of the individual components. In the case of the multipole expansion, on the other hand, the parameters of the basic dipole are easily interpreted, but the structure created by the higher multipole components is more difficult to judge (Euchner et al. 2002). The hybrid models correspond to special situations not encountered in truncated multipole expansions of low  $l_{\max}$ , and we lack information from dynamo theory on the feasibility of such models. For the sake of economy and simplicity of presentation, we present results for the offset dipole as a simple and popular model and for the full multipole expansion for either  $l_{\max} = 3$  or 5, with occasional comments on other models (a multipole expansion up to  $l_{\max} = 4$  was not tested). We use two graphic forms to present the results: (i) the “ $B - \psi$  diagrams” that depict the frequency distribution of field vectors over the surface of the star at a given orbital phase in the  $B - \cos \psi$  plane; and (ii) actual images of the field distribution. The latter include (a) the field strength  $B$ , (b)  $\cos \psi = B_l/B$  with  $B_l$  the field component along the line of sight, and (c) an image of the maximum radial distance to which a field line extends that originates from a certain location on the star. We subjected the flux and polarization spectra at all orbital phases simultaneously to the tomographic analysis, weighing all wavelengths equally except for narrow intervals around the Balmer emission lines. An improved fit can be obtained by restricting it to the set of flux and polarization spectra at a single phase, but if the model parameters deduced for different phases disagree, there is no unique solution (Euchner et al. 2006).

#### 4. Results

The models are fitted to the average flux and circular polarization spectra in four orbital phase bins for EF Eri, five bins for BL Hyi, and three bins for the half orbit of CP Tuc. The orbital phase conventions used in this paper are the dip ephemeris for EF Eri (Piirola et al. 1987a), slightly updated by including the ROSAT PSPC dip timings from July 1990<sup>1</sup> (Beuermann et al. 1991), the ephemeris for the start of the bright phase for BL Hyi (Wolff et al. 1999), and the dip ephemeris for CP Tuc (Ramsay et al. 1999). In our previous papers on the field structure of single white dwarfs, we considered the inclination of the line of sight relative to the rotation axis as a free parameter of the fit. For the mCVs, however, independent and better information on  $i$  is available from the light curve and broad band polarization

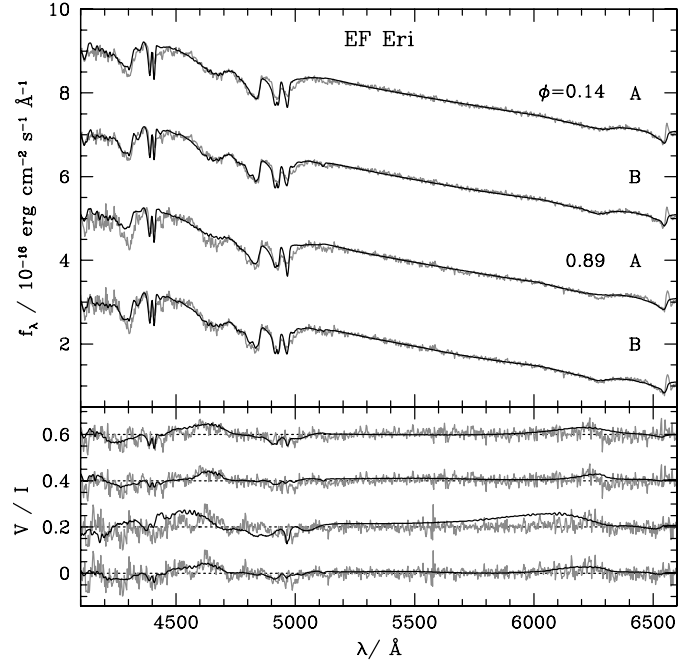


**Fig. 1.** Flux spectra (top) and circular polarization spectra (bottom) of EF Eri at two selected orbital phases and for two field models. Model A is an offset dipole and model B a multipole expansion truncated at  $l_{\max} = 5$ . The data are shown as grey curves, the best-fit models from the Zeeman tomographic analysis are overlaid as solid black curves. The order of orbital phases and field models for the polarization spectra is the same as for the flux spectra, i.e., the bottom spectrum and third from the bottom are for the multipole expansion, the other two for the offset dipole. The ordinate scales refer to the bottom spectrum, the other ones are arbitrarily shifted upwards.

studies in their high states. We use  $i = 55^\circ$  for EF Eri (Piirola et al. 1987b; Achilleos et al. 1992) and  $i = 40^\circ$  for CP Tuc (Thomas & Reinsch 1996; Ramsay et al. 1999). For BL Hyi, we use  $i = 32^\circ$  (Schwope et al. 1995).

Our Zeeman tomography uses the observed flux and circular polarization spectra of all orbital phases. For conciseness, however, we show the spectra only for two selected phases and the globes representing the field structure only for  $\phi \simeq \phi_0$  when the main accretion spot most directly faces the observer, i.e.,  $\phi_0 \simeq 0.10$  for EF Eri,  $\phi_0 \simeq 0.20$  for BL Hyi, and probably  $\phi_0 \simeq 0.50$  for CP Tuc. Our phases closest to  $\phi_0$  are  $\phi = 0.14$  for EF Eri,  $\phi = 0.19$  for BL Hyi, and  $\phi = 0.43$  for CP Tuc.

Figures 1 and 2 show the flux and circular polarization spectra (grey curves) for the value of  $\phi$  closest to  $\phi_0$  and for another phase selected to point out differences in the Zeeman spectra. The spectral data in Figs. 1 and 2 are shown twice along with the best-fit theoretical spectra for two models, the shifted dipole (model A) and the multipole expansion with  $l_{\max} = 3$  or 5 (model B). The ordinate scales refer to the bottom spectra, the other ones being shifted upwards by arbitrary amounts. Since the fit to  $H\alpha \sigma^+$  always mimics that of the  $\sigma^-$  feature, we have omitted the former in the figures to avoid excessive compression in wavelength. That feature is included in the fits, however.

We judged the fits by eye and by a formal global  $\chi^2$  for the flux and polarization spectra at all phases combined and with all wavelengths weighted equally. As discussed by Euchner et al. (2005), the formal reduced  $\chi^2_v$  are large because the adjustment of the observed continua to the model continua is not perfect and the standard deviations used in calculating  $\chi^2$  account for the statistical noise in the data but not for the remaining

<sup>1</sup> The updated EF Eri dip ephemeris with 90% confidence errors is  $T_0 = \text{HJD } 244\,3944.9518(6) + 0.056265949(14) E$ .

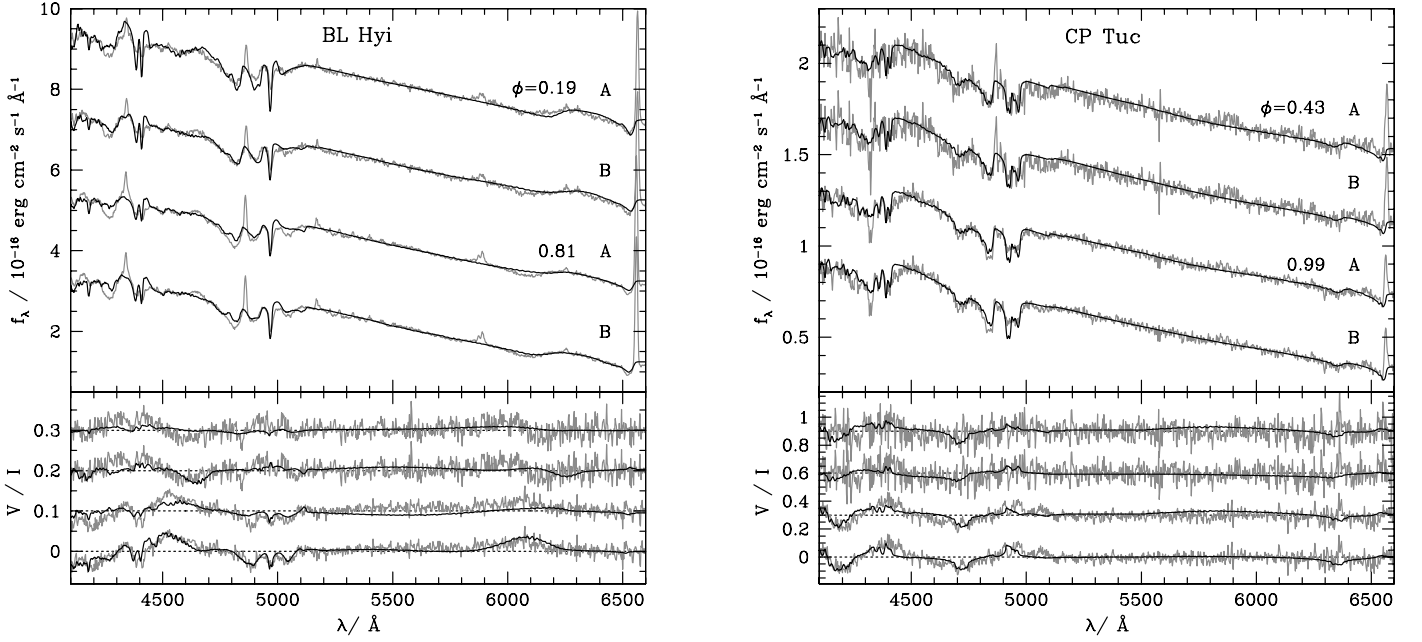


**Fig. 2.** As Fig. 1, but for BL Hyi and CP Tuc. Model A is an offset dipole and model B a multipole expansion truncated at  $l_{\max} = 3$ .

**Table 2.** Best-fit magnetic parameters for the truncated multipole expansions up to degree  $l_{\max} = 5$  for EF Eri and up to  $l_{\max} = 3$  for BL Hyi and CP Tuc. The coefficients  $g_l^m$  and  $h_l^m$  are in MG. The tilt angle of the multipole axis relative to the rotational axis is  $74^\circ$ ,  $32^\circ$ , and  $23^\circ$  for EF Eri, BL Hyi, and CP Tuc, respectively.

$m$		EF Eri					BL Hyi			CP Tuc		
		$l = 1$	2	3	4	5	$l = 1$	2	3	$l = 1$	2	3
0	$g_l^0$	-5.9	4.2	4.1	-1.9	-0.3	-5.2	-12.0	5.8	3.5	14.6	-1.6
1	$g_l^1$	6.1	-4.8	1.2	1.0	-0.4	-8.1	15.8	-2.5	-15.5	8.5	-2.8
	$h_l^1$	0.7	12.7	-1.2	0.2	4.9	0.2	12.8	6.6	8.1	-13.0	4.9
2	$g_l^2$		10.8	-3.9	-4.0	-1.6		12.5	-2.7		-3.7	-1.5
	$h_l^2$		-1.0	5.4	-5.8	2.1		-10.4	-2.1		0.3	-1.7
3	$g_l^3$			7.7	-2.0	-0.9			-2.5			-4.9
	$h_l^3$			1.8	-5.1	-0.6			8.6			0.0
4	$g_l^4$				2.4	-0.2						
	$h_l^4$				1.5	3.7						
5	$g_l^5$					-1.2						
	$h_l^5$					3.2						

systematic differences between model and data. We quote the global  $\chi^2_\nu$  values that serve as a guideline, but also judge the merits and failures of individual models by eye and describe them in words. Not surprisingly, significantly reduced  $\chi^2_\nu$  are obtained by excluding the poorly fitting spectral regions from the fit. However, since these regions differ from object to object, we have refrained from including such restrictions in a general way. We have assured ourselves, however, that the inclusion of the poorly fitting regions does not affect the selection of the best-fitting model as the one with the lowest  $\chi^2_\nu$ .

For all three objects, the dipole, even after allowing for an off-center shift in the three spatial coordinates, does not provide a good fit, whereas the multipole expansions fare decidedly better. While it is possible that substantially more complicated hybrid models might be successful, we are limited in the number of models that could be tested by the slow convergence properties of our code (see Sect. 5). We quote some of the parameters of the dipole models in the text and list the coefficients  $g_l^m$  and  $h_l^m$  of the best-fit multipole expansions (Euchner et al. 2006) in Table 2. These coefficients are given in MG, and, although such models are difficult to visualize, the numbers allow some insight into the

field structure: the three  $l = 1$  coefficients combine to define the dipole, which is allowed to be inclined relative to the multipole axis; the  $l, m = 2, 0$  coefficient describes the quadrupole aligned along the multipole axis and the following  $m = 0$  coefficients the octupole and higher multipole zonal components; the  $m \neq 0$  (tesseral) components are modulated in azimuth in addition to zenith angle.

Figures 3 to 5 contain the representations of the field structure at  $\phi \approx \phi_0$  for both the offset dipole and the multipole expansions. In these figures, progressing phase corresponds to anti-clockwise rotation and a motion of a feature on the globes from left to right. The most probable field strength seen at the face when the prospective accretion spot faces the observer and the range of field strength over the whole star are listed in Table 3. We discuss the results in these figures and tables with each object below.

#### 4.1. EF Eri

The main accretion region in EF Eri faces the observer near phase  $\phi = 0.10$  and is located  $\sim 30^\circ$  from the rotational axis

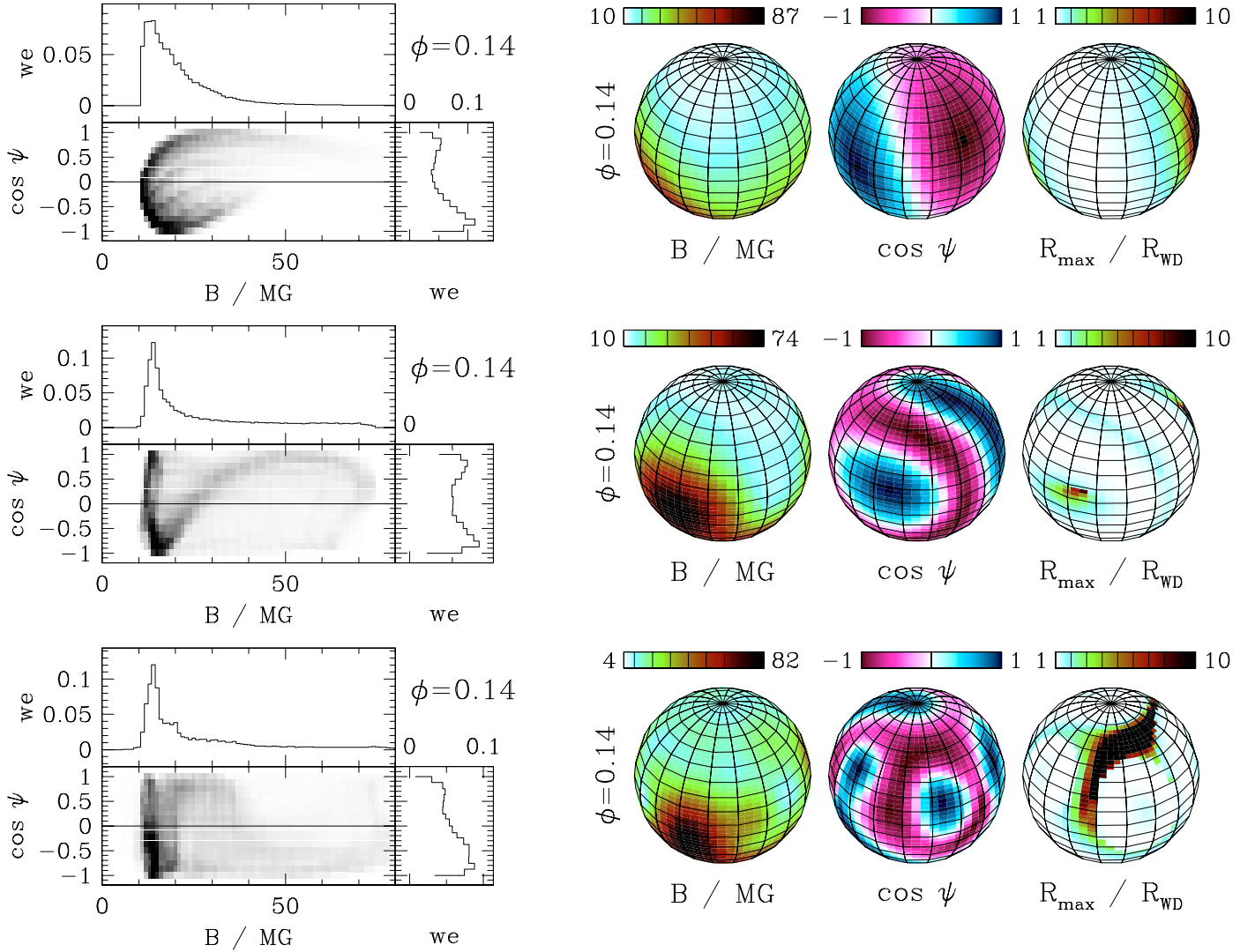


**Fig. 3.** Visualization of the three magnetic field models discussed for EF Eri. The results shown are for orbital phase  $\phi = 0.14$  near the peaks of the X-ray and infrared cyclotron fluxes and shortly past the infrared absorption dip ( $\phi = 0$ ). The models are (i) the offset dipole (top), (ii) the full multipole expansion truncated at  $l_{\max} = 3$  (center), and (iii) the same for  $l_{\max} = 5$  (bottom). The left panels show the  $B - \psi$  diagrams in which the frequency distribution of field vectors over the surface is represented by a grey scale. Also shown are the weight distributions (we) projected onto the  $B$  and the  $\cos \psi$  axes. The right panels display globes with the distributions of the absolute value of the field strength  $B$ , of  $\cos \psi = B_l / B$  with  $B_l$  the field component along the line of sight, and of the maximum radius in units of  $R_{WD}$  to which the field lines extend. Lines reaching  $10 R_{WD}$  were not followed further out. The color bars above the globes indicate the range of the respective parameters over the visible hemisphere (see the online version of the paper for colored figures). Progressing orbital phase corresponds to an anti-clockwise rotation of the globes.

(Beuermann et al. 1987; Pirola et al. 1987b). The field strength in the accretion spot is low, as indicated by the featureless optical cyclotron continuum. Zeeman halo absorption in the ordinary ray of the cyclotron continuum (Oestreich et al. 1990) and cyclotron humps in the infrared (Ferrario et al. 1996; Harrison et al. 2004; Howell et al. 2006) suggest a field in the range of 10 to 21 MG with different studies favoring different values. The positive circular polarization in the high state (Pirola et al. 1987b; Oestreich et al. 1990) implies that the accreting field line in the main (X-ray emitting) spot points away from the observer (negative  $\cos \psi$ ). There is evidence from spectropolarimetry (Oestreich et al. 1990) and from broad band polarimetry (Pirola et al. 1987b) that a second accretion region is located near the same meridian at a colatitude of about  $115^\circ$  (lower hemisphere) with a disputed polarity. While Pirola et al. (1987b) argue for the same polarity as the main spot, Oestreich et al. (1990) favor opposite polarity. Both accretion regions

are only about  $80^\circ$  apart, an observation that led Meggitt & Wickramasinghe (1989) to suggest a quadrupole field.

The best-fit offset dipole (model A in Fig. 1 and top panels in Fig. 3) has a polar field strength (of the unshifted dipole) of 44.0 MG, is inclined to the rotation axis by  $75^\circ$ , and is shifted off center by  $x_d$ ,  $y_d$ , and  $z_d$  equaling 0.26,  $-0.01$ , and  $-0.17 R_{WD}$ , respectively, with  $R_{WD}$  the white dwarf radius. The  $z$ -offset is directed along the dipole axis and  $x$  and  $y$  denote perpendicular directions (Euchner et al. 2002). A moderately good fit at  $\phi = 0.14$  is accompanied by an utter failure at  $\phi = 0.89$  with a global  $\chi^2_\nu = 19.97$ . This is seen in the  $H\alpha$  and  $H\beta$   $\sigma^-$  features in the flux spectrum of Fig. 1 at 4800 and 6100 Å, and in the polarization spectrum at all wavelengths. As an added disadvantage, the model lacks open field lines at the position of the accretion spot near the meridian in the upper hemisphere at  $\phi = 0.14$  (Fig. 3, top panel). As expected, setting the shifts perpendicular to the axis equal to zero does not improve the situation. More



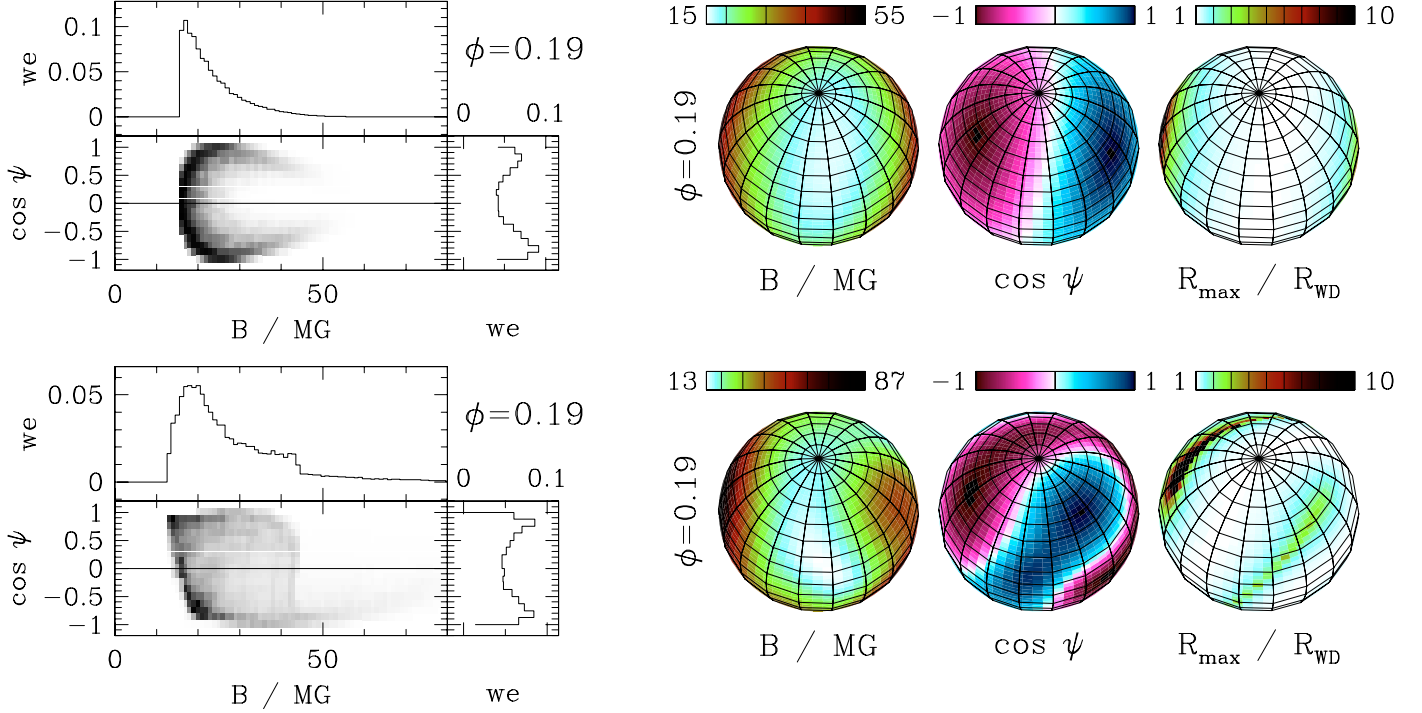


**Fig. 4.** Visualization of the two magnetic field models discussed for BL Hyi, the offset dipole (*top*) and the  $l_{\max} = 3$  multipole expansion (*bottom*), both shown for orbital phase  $\phi = 0.19$  with the main accretion region on the lower hemisphere in front. The  $B - \psi$  diagrams are on the left and the model field distributions on the right. Further details are as in Fig. 2.

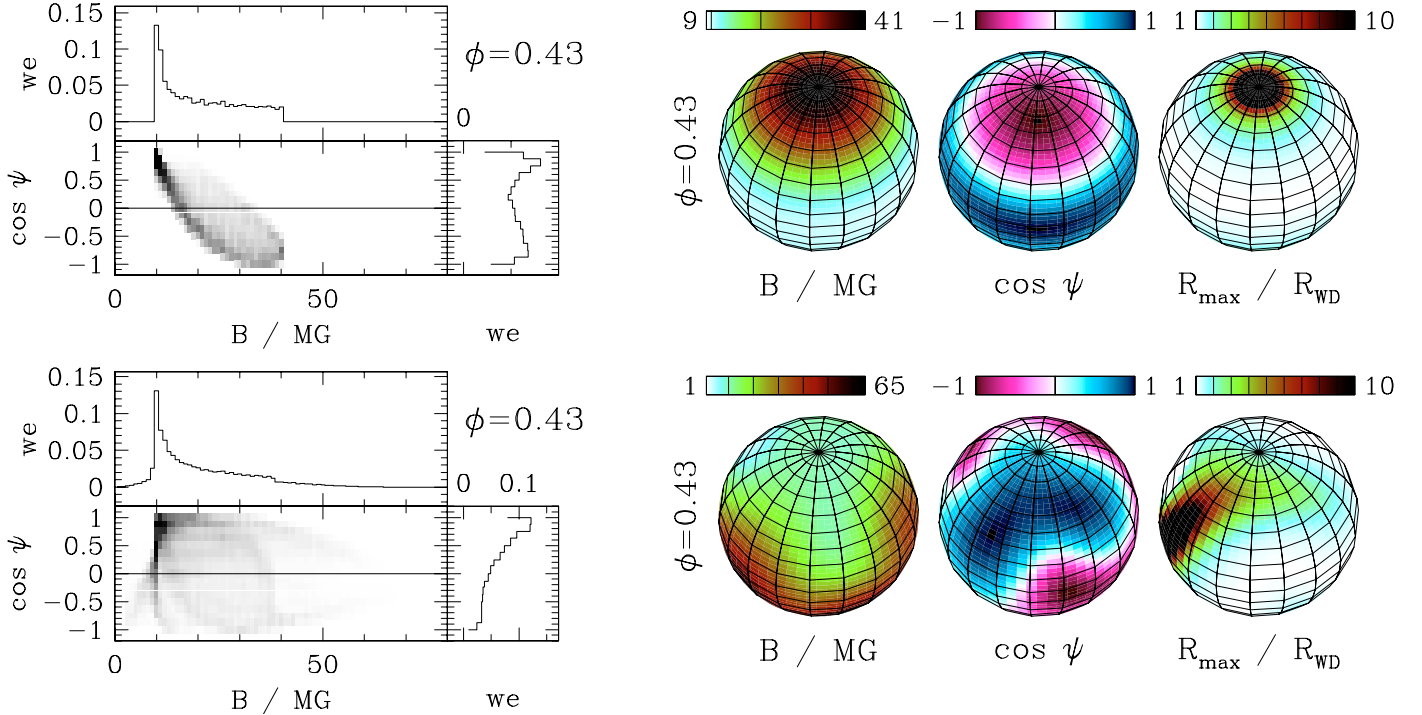


**Fig. 5.** Visualization of the two magnetic field models discussed for CP Tuc, the offset dipole (*top*), and the  $l_{\max} = 3$  multipole expansion (*bottom*), both shown for orbital phase  $\phi = 0.43$  with the main accretion region on the lower hemisphere in front. The  $B - \psi$  diagrams are on the left and the model field distributions on the right. Further details are as in Fig. 2.

complex hybrid models of aligned dipole, quadrupole, and octupole, either centered or off-centered, did not fare well either. Our fits quite reliably exclude this class of models.

Of the multipole expansions up to  $l_{\max} = 3$  (with 15 fit parameters) and  $l_{\max} = 5$  (with 35 fit parameters), the latter yields a slightly better fit with  $\chi^2_{\nu} = 13.99$  vs. 14.88 for the former. The

$l_{\max} = 5$  case is shown in Fig. 1 as model B. There are some subtle differences resulting in a better fit of either model to one or the other spectral feature and, in summary, one would have to conclude that there is no good basis for including the added parameters of the  $l_{\max} = 5$  model, if judgment is based solely on the flux and polarization spectra. In line with this, we find that the

**Table 3.** Dipole field strength  $B_{\text{dip}}$ , most frequent photospheric field strength  $B_{\text{prob}}$ , and ranges  $B_{\text{min}}$  to  $B_{\text{max}}$  in the models of EF Eri, BL Hyi, and CP Tuc in MG. The former refers to the orbital phase when the accretion spot faces the observer (Fig. 3–5), the latter to all orbital phases combined.

Object	Model	$B_{\text{dip}}$	$B_{\text{prob}}$	$B_{\text{min}}$	$B_{\text{max}}$
EF Eri	offset dipole	44.0	12	10	110
	$l_{\text{max}} = 5$ multipole		13	4	111
BL Hyi	offset dipole	59.5	17	15	88
	$l_{\text{max}} = 3$ multipole		18	13	110
CP Tuc	offset dipole	19.8	10	9	41
	$l_{\text{max}} = 3$ multipole		10	1	69

$B - \psi$  diagrams in Fig. 3 (center panel for  $l_{\text{max}} = 3$ ; bottom panel for  $l_{\text{max}} = 5$ ) are similar in the predominance of field strengths of 10–15 MG, but differ in the extensions to higher field strengths. The decisive difference of the two multipole expansions is depicted in the rightmost globes in Fig. 3. The  $l_{\text{max}} = 3$  model possesses only a small spot from which field lines reach far out. Such field lines, whether they close within the Roche lobe of the white dwarf or not, are needed for the accretion stream to be guided towards the white dwarf. The field in this tiny spot is directed outward ( $\cos \psi > 0$ ), however, leading to negative polarization of the cyclotron emission from this potential accretion spot, while the observed polarization is positive ( $\cos \psi < 0$ ). The  $l_{\text{max}} = 5$  model, for comparison, displays a large arc-like region of ingoing field lines, which also covers the expected location of the primary accretion region  $\sim 30^\circ$  from the rotation axis and facing the observer shortly past  $\phi = 0$  (Beuermann et al. 1987; Pirola et al. 1987b). This ribbon of open ingoing field lines with  $\cos \psi < 0$  winds around a region of quadrupole-like low-lying magnetic arcs in the lower right quadrant at  $\phi = 0.14^2$ . The decisive point in favor of the  $l_{\text{max}} = 5$  truncated multipole expansion among the models studied is the correct polarity of the open field lines with  $\cos \psi < 0$  and a positive sign of the resulting circular polarization of the high-state cyclotron emission from the main accretion spot.

As seen from Table 2, the dipole component of the multipole expansion is relatively weak, with a polar field strength of 8.5 MG obtained by squaring the three dipole coefficients. The strongest components are azimuthally modulated quadrupole-like ones. All individual  $l = 3$ –5 coefficients are smaller than 10 MG, but their combined effect is significant in shaping the field structure (Fig. 3), which is not that of an  $m = 0$  quadrupole. Hence, from the present study, we conclude that the field structure of EF Eri is substantially more complex than that of a centered or offset dipole or quadrupole and may be even more complex than suggested by the present best fit.

#### 4.2. BL Hyi

BL Hyi is another polar that displays a complex accretion geometry, usually referred to as “one-pole” and “two-pole” accretion in states of low and high accretion rates, respectively (Beuermann & Schwope 1989). The main hard X-ray and cyclotron emitting accretion spot is located in the lower hemisphere of the white dwarf and is visible only for part of the orbit. Its appearance at the limb of the white dwarf defines photometric phase  $\phi = 0$ . It slowly disappears some 0.40 phase units later (Pirola et al. 1987a). The second emission region in the upper

hemisphere facing the observer emits in the soft X-ray and EUV regime and is visible over much of the orbital period (Schwope & Beuermann 1993; Szkody et al. 1997). The sign of the circular polarization of the cyclotron emission from the main (second) pole is negative (positive) implying positive (negative)  $\cos \psi$  (Cropper 1987; Bailey 1988; Schwope & Beuermann 1989). The dominant photospheric field strength is 22 MG, but the presence of significantly higher fields is inferred from Zeeman spectroscopy. A field of only 12 MG was at times detected by H $\alpha$  Zeeman absorption in the cyclotron continuum emission of the main accretion spot (Schwope et al. 1995), but the feature may have originated at some height above the white dwarf surface.

Our present data cover the whole binary orbit in five about equally spaced intervals. The best-fit offset dipole model features a polar field strength of 59.5 MG, an inclination against the rotation axis of  $80^\circ$ , and offsets of  $-0.18$ ,  $0.15$ , and  $-0.03 R_{\text{WD}}$  in  $x$ ,  $y$ , and  $z$ . As in the case of EF Eri, the offset dipole model does not fare well. We find  $\chi^2_{\nu} = 200.3$ , which is so large because of the small standard deviation in the low-noise observed spectrum and obviously poor fits in a few places. The model fails to reproduce the H $\alpha$   $\sigma^-$  feature in the flux spectra near 6000 Å and also much of the detail in the circular polarization spectra over the entire wavelength range (Fig. 2, left panel). The fit to the polarization data is particularly poor at  $\phi = 0.40$  (not shown). We discard the offset dipole model because it provides a comparatively poor fit and because of the lack of open field lines in both the upper and the lower hemisphere at  $\phi = 0.19$  at positions that might correspond to the main and the secondary accretion regions (Fig. 4, upper right).

The multipole expansion truncated at  $l_{\text{max}} = 3$  fits better than the offset dipole, although there are still some systematic deviations in the flux and circular polarization spectra, in particular near 4300 Å, as well as 6050 Å and around 5500 Å. In spite of the still very high  $\chi^2_{\nu} = 193.51$ , the field distribution looks promising. On the positive side, we note the correct representation of the reversal of the polarization near 4600 Å between  $\phi = 0.19$  and  $\phi = 0.81$  and the approximately correct description of the H $\alpha$   $\sigma^-$  polarization near 6100 Å. As in the case of EF Eri, the quadrupole-like components are strongest, but, again, the other components are essential for the field structure (Table 2). There is a longish ribbon of field lines reaching out moderately far (about  $3 R_{\text{WD}}$ ). It faces the observer near  $\phi = 0.19$  and yields negative circularly polarized cyclotron emission (positive  $\cos \psi$ ) as required for the main accretion region. A second region with negative  $\cos \psi$  may allow access as close as  $35^\circ$  from the rotational pole and may be responsible for the intense flaring soft X-ray emission (Schwope & Beuermann 1989) and the positive circularly polarized cyclotron emission at orbital phases when the main spot is behind the white dwarf. The  $B - \psi$  diagram prominently shows field strengths between 13 and 45 MG with a faint (and ill-defined) extension to beyond 100 MG. The ribbon that may contain the main accretion spot crosses the 13 MG field minimum, quite consistent with the featureless cyclotron continuum and the 12-MG Zeeman absorption in the cyclotron emission of the main spot. These facts suggest that the model approaches reality, although the large  $\chi^2_{\nu}$  lets us suspect that the final model is still different. The experience from EF Eri with substantially different structures of the best-fit multipole expansions for  $l_{\text{max}} = 3$  and  $l_{\text{max}} = 5$  suggests that such an improved model can be found. In this case, however, convergence problems have prevented the construction of an  $l_{\text{max}} = 4$  or 5 model. We do not expect such a better-fitting model to possess a simpler structure than the  $l_{\text{max}} = 3$  model and conclude that BL Hyi possesses a

<sup>2</sup> The interested reader may look up Fig. 7 of Schwope et al. (1995), which shows the field structure of such a region at its upper pole.



complex field geometry, probably not completely unraveled with the model presented here.

#### 4.3. CP Tuc

Unlike the majority of polars, CP Tuc was discovered by its hard X-ray emission (Misaki et al. 1996). It displays a broad dip in the X-ray flux that was used to derive a rotational ephemeris of the white dwarf (Ramsay et al. 1999). The narrow emission line from the heated face of the secondary star yields the orbital period (Thomas & Reinsch 1996), which agrees with the rotational period proving synchronism. The ephemeris of these authors shows that inferior conjunction of the secondary star occurs at dip phase  $\phi = 0.08$ . There is debate about the location of the accretion region: Misaki et al. (1996) suggested that the energy-dependent X-ray dip arises from photoabsorption, while Ramsay et al. (1999) assign it to a self-eclipse by the white dwarf. In the first case, the accretion spot conveniently faces the observer shortly before inferior conjunction; in the latter it faces away from the secondary.

As noted above, our data cover only one half of the binary orbit. They were combined into two sets of flux and polarization spectra at dip phases  $\phi = 0.99$  and  $0.21$ , plus a noisier single set at  $\phi = 0.43$ . In the Misaki et al. (1996) and Ramsay et al. (1999) interpretations, the accretion spot faces the observer near  $\phi = 0$  and  $\phi \simeq 0.55$ , respectively. We show our spectra at  $\phi = 0.99$  and  $\phi = 0.43$  in Fig. 2 (right panel). Model A is the offset dipole and model B the multipole expansion with  $l_{\max} = 3$ , of which the latter yields a formally better fit with  $\chi^2_{\nu} = 12.35$  and  $11.78$ , respectively. Visual inspection, however, shows that the differences are not pronounced and that both models reproduce the major Zeeman features of H $\beta$  and the higher Balmer lines in the flux and the polarization spectra reasonably well. The  $B - \psi$  diagrams in Fig. 5 demonstrate the preponderance of field strengths close to 10 MG, which make CP Tuc a low-field polar and may explain the hard X-ray spectrum. The offset dipole has a polar field strength of 19.8 MG, is practically aligned with the rotation axis, and offset mainly in  $z$  by  $0.21 R_{\text{WD}}$ . It has its high-field pole in the upper hemisphere, whereas the multipole model possesses low fields in the same region. The dipole component of the multipole expansion has a polar field strength of 17.8 MG, but the quadrupole-like components are of similar strength and the octupole-like components are non-negligible (Table 2). Both models, offset dipole and multipole expansion, differ in the sign of the longitudinal field component over the near and far hemispheres. The featureless cyclotron continuum indicates a low field strength (Thomas & Reinsch 1996), and the negative circular polarization of the continuum (Ramsay et al. 1999) shows that the accretion region must lie in the lower (upper) hemisphere for the dipole (multipole) model. Only the multipole model, however, possesses an extended region of outgoing field lines that faces the observer near  $\phi = 0.55$ , as expected from the Ramsay et al. (1999) model (some  $0.12$  in phase later than in the lower right globe of Fig. 5). In summary, CP Tuc is the third of the polars studied here with a field structure more complex than a simple offset dipole. As a caveat we recall the incomplete phase coverage. The results for CP Tuc are, therefore, preliminary.

##### 4.3.1. Summary of results

For all three objects, the truncated multipole expansions yield significantly better fits than the offset dipole models. Only the former provide access to the surface of the white dwarf via field lines reaching sufficiently far out at the expected positions on the surface. As seen from Table 3, dipole and multipole

models have practically the same most frequent values of the field strength. They also cover similar ranges, in particular, if one considers that the faint extensions in the probability distribution to the lowest and highest field strengths are not well defined. This similarity reflects the fact that both models more or less fit the principal features of the Zeeman spectra. Intuitively, one might consider rotating the offset dipole model to match the accretion conditions, but that changes the phase-dependent  $B - \psi$  diagrams and destroys the fits to the Zeeman spectra. Hence, the offset dipoles clearly cannot match all conditions simultaneously. In spite of the similar  $B$ -distributions, the field structures of the two models are significantly different and our conclusion in favor of structures more complex than offset dipoles is safe.

## 5. Discussion

We have presented the first Zeeman tomographic study of the field structure of white dwarfs in polars based on phase-resolved VLT spectropolarimetry. We have demonstrated that the studied stars possess field structures significantly more complex than simple centered or offset dipoles. Such a result was considered possible or even likely in many previous publications, but detailed proof had not been available so far. Our results clearly demonstrate this complexity, although we have to caution that our best fits may not yet describe reality in every detail. The simplest parameter indicative of a structure more complex than a centered dipole is the range of field strengths over the surface of the star that exceeds seven for the best-fit models for all three stars, while it would be two for a centered dipole. The presence of strong higher multipole components besides the dipole may be surprising considering the fact that the white dwarfs in CVs have a typical age in excess of 1 Gyr (Kolb & Baraffe 1999), sufficient to expect substantial decay of the higher order components (e.g., Cumming 2002). Recreation of higher order poloidal components from a toroidal interior field has been suggested by Muslimov et al. (1995), but it is not known whether the required strong toroidal field exists in magnetic white dwarfs. The single white dwarfs HE 1045-0908 and PG 1015+014 (Euchner et al. 2005, 2006) have similarly complex magnetic field structures at an age of  $\sim 0.5$  Gyr. At present, field evolution is not sufficiently constrained by observations, but may become so when the field structure of more objects becomes available.

We find that fitting the field structure of accreting white dwarfs in CVs offers a decisive advantage over the analysis of isolated white dwarfs. The location of the accretion spot and the absolute value and direction of the field vector in the spot can be deduced independently, e.g., from X-ray and optical light curves and from broad band polarimetry. Requiring that a successful field model complies with this independent information turns out to be a powerful tool and is the main driver for our conclusion in favor of a field structure more complex than an offset dipole in all three objects.

There is a semantic aspect worth mentioning. A comparison of the right-hand globes for the multipole expansions and the offset dipoles in Figs. 3–6 (including the phases omitted for conciseness) demonstrates that the latter have well-defined circular regions of outgoing field lines that are properly addressed as ‘poles’. The corresponding regions in the multipole structures, on the other hand, are quite irregular and longish structures that imply accretion geometries which probably allow access to the white dwarf surface at more than one position characterized by a wide range of angular separations. The resulting accretion geometry is no longer appropriately described by the dipole-inspired expressions “one-pole accretion” or “two-pole accretion”.

Given the complicated field structures in the three polars studied here, it is desirable to extend the Zeeman tomographic analysis to a larger number of objects to distinguish between idiosyncrasies of individuals and the general properties of the class. Such a program is feasible, but it calls also for a consideration of the limitations of our approach. One obvious limiting factor is telescope time. Although we have typically used two orbital periods of high signal-to-noise spectra using the VLT and the spectropolarimetric capabilities of FORS1, the remaining noise in the circular polarization spectra limits the discrimination between the  $B - \psi$  diagrams of different models. A more extensive tomographic program requires covering several orbital periods of each target with an 8-m class telescope. A second limiting factor is CPU time. To thoroughly test a given field model, 50 to 100  $\chi^2$ -minimization runs are typically required because they tend to get stuck in secondary minima of the complicated  $\chi^2$  landscape. Each step in this process requires assembling the Zeeman spectra for the respective field model from the database. The resulting lack of speed is the main reason why we had to limit the number of models tested.

In the previous papers of this series (Euchner et al. 2005, 2006), we have already discussed the alternative approach of Donati et al. (1994), the Zeeman Broadening Analysis (ZEBRA). This method determines the best-fitting  $B - \psi$  diagrams for each orbital phase interval directly from the data, employing the Maximum Entropy Method (MEM) as a regularization procedure. The advantage is predictably speed, the disadvantage is the uncertainty whether the individual  $B - \psi$  diagrams are compatible with any global physical field model. The method faithfully reproduces the distribution in the absolute value of  $B$  over the visible hemisphere at a given orbital phase, but substantially smears the angle relative to the line of sight (Donati et al. 1994). If interpreted in terms of a multipole model, the reconstructed  $B - \psi$ -diagram then leads to spurious higher multipole components. Furthermore, the requirement that the so-derived diagrams contain the  $B - \psi$  combination describing the accretion spot is easily implemented, but the exact location of the spot on the star is not because the method forgoes imaging. On the other hand, testing a larger number of field models for compatibility with the  $B - \psi$  diagrams for the individual phase intervals will probably be less time consuming than our present approach because the large database of Zeeman spectra need no longer be accessed after these diagrams have been established. We plan to study the different approaches further to find the ultimately preferable one.

**Acknowledgements.** This work was supported in part by BMBF/DLR grant 50 OR 9903 6. B.T.G. was supported by a PPARC Advanced Fellowship.

## References

- Achilleos, N., Wickramasinghe, D. T., & Wu, K. 1992, MNRAS, 256, 80
- Araujo-Betancor, S., Gänsicke, B. T., Long, K. S., et al. 2005, ApJ, 622, 589
- Bailey, J. 1988, in Polarized Radiation of Circumstellar Origin, Vatican Observatory, ed. G. V. Coyne et al., 105
- Beuermann, K., & Schwöpe, A. D. 1989, A&A, 223, 179
- Beuermann, K., Stella, L., & Patterson, J. 1987, ApJ, 316, 360
- Beuermann, K., Thomas, H.-C., & Pietsch, W. 1991, A&A, 246, L36
- Beuermann, K., Wheatley, P., Ramsay, G., Euchner, F., & Gänsicke, B. T. 2000, A&A, 354, L49
- Cumming, A. 2002, MNRAS, 333, 589
- Cropper, M. 1987, MNRAS, 228, 389
- Donati, J. F., Achilleos, N., Matthews, J. M., & Wesemael, F. 1994, A&A, 285, 285
- Euchner, F., Jordan, S., Beuermann, K., Gänsicke, B. T., & Hessman, F. V. 2002, A&A, 390, 633
- Euchner, F., Reinsch, K., Jordan, S., Beuermann, K., & Gänsicke, B. T. 2005, A&A, 442, 651
- Euchner, F., Jordan, S., Beuermann, K., Reinsch, K., & Gänsicke, B. T. 2006, A&A, 451, 671
- Ferrario, L., Bailey, J., & Wickramasinghe, D. 1996, MNRAS, 282, 218
- Harrison, T. E., et al. 2004, ApJ, 614, 947
- Howell, S. B., Walter, F. M., Harrison, T. E., et al. 2006, ApJ, 652, 709
- Kolb, U., & Baraffe, I. 1999, MNRAS, 309, 1034
- Krzeminski, W., & Serkowski, K. 1977, ApJ, 216, L45
- Meggitt, S. M. A., & Wickramasinghe, D. T. 1989, MNRAS, 236, 31
- Misaki, K., Terashima, Y., Kamata, Y., Ishida, M., Kunieda, H., & Tawara, Y. 1996, ApJ, 470, L53
- Muslimov, A. G., Van Horn, H. M., & Wood, M. A. 1995, ApJ, 442, 758
- Oestreicher, R., Seifert, W., Wunner, G., & Ruder, H. 1990, ApJ, 350, 324
- Pirola, V., Coyne, G. V., & Reiz, A. 1987a, A&A, 185, 189
- Pirola, V., Coyne, G. V., & Reiz, A. 1987b, A&A, 186, 120
- Ramsay, G., Potter, S. B., Buckley, D. A. H., & Wheatley, P. J. 1999, MNRAS, 306, 809
- Schwöpe, A. D., & Beuermann, K. 1989, A&A, 222, 132
- Schwöpe, A. D., & Beuermann, K. 1993, Cataclysmic Variables and Related Physics, 2nd Technion Haifa Conference, ed. O. Regev, & G. Shaviv, Annals of the Israel Physical Society, 10, 234
- Schwöpe, A. D., Beuermann, K., & Jordan, S. 1995, A&A, 301, 447
- Szkody, P., Vennes, S., Sion, E. M., Long, K. S., & Howell, S. B. 1997, ApJ, 487, 916
- Szkody, P., Harrison, T. E., Plotkin, R. M., et al. 2006, ApJ, 646, L147
- Thomas, H.-C., & Reinsch, K. 1996, A&A, 315, L1
- Wickramasinghe, D. T., & Ferrario, L. 2000, PASP, 112, 873
- Wolff, M. T., Wood, K. S., Imamura, J. N., Middleditch, J., & Steiman-Cameron, T. Y. 1999, ApJ, 526, 435